Experimental and Computational Models for Side Chain Discrimination in Peptide–Protein Interactions

Anna Lidskog,[a] Sami Dawaigher,[a] Carlos Solano Arribas,[a] Anna Ryberg,[a] Jacob Jensen,[a] Karl Erik Bergquist,[a] Anders Sundin,[a] Per-Ola Norrby,*[b] and Kenneth Wärnmark*[a]

Abstract: A bis(18-crown-6) Tröger's base receptor and 4-substituted hepta-1,7-diyl bisammonium salt ligands have been used as a model system to study the interactions between non-polar side chains of peptides and an aromatic cavity of a protein. NMR titrations and NOESY/ROESY NMR spectroscopy were used to analyze the discrimination of the ligands by the receptor based on the substituent of the ligand, both quantitatively (free binding energies) and qualitatively (conformations). The analysis showed that an all-*anti* conformation of the heptane chain was preferred for most of the ligands, both free and when bound to the receptor, and that for all of the receptor-ligand complexes, the substituent was located inside or partly inside of the aromatic cavity of the receptor. We estimated the free binding energy of a methyl- and a phenyl group to an aromatic cavity, via CH-π, and combined aromatic CH-π and π-π interactions to be −1.7 and −3.3 kJ mol^{-1}, respectively. The experimental results were used to assess the accuracy of different computational methods, including molecular mechanics (MM) and density functional theory (DFT) methods, showing that MM was superior.

Introduction

Protein-ligand interactions play a crucial role in a number of essential biochemical processes, including cell regulation, signaling and transmembrane transport.[1,2] The intermolecular forces involved in such interactions include hydrogen bonding, hydrophobic, ion-ion and ion-dipole interactions, and van der Waals forces.[3] Also included are interactions involving aromatic groups, such as π-π[4–8] and CH-π interactions.[6,9–11] One important type of protein-ligand interaction is the interaction between proteins and short peptide sequences,[12–14] which has been implicated as a potential drug target.[15–17] As such, the development of model systems where such interactions can be studied under controlled conditions are of high interest.

One way of predicting and modeling the interactions between proteins and peptides is computational chemistry. In recent years, computational methods have been extensively used in medicinal chemistry, enabling virtual screening and drug design.[18–22] A key issue for computational chemistry is how to validate the accuracy and quality of different computational methods. To this end, the benchmarking of computational methods against experimental results is of high importance.[23] Experiments aimed to be used to benchmark theory need to be carefully designed and must generate results of high quality.

In this study, we have constructed a model system consisting of a receptor with an aromatic cavity and a number of ligands bearing different substituents, in order to model the interactions between the side chain of a peptide and an aromatic region of a protein. The receptor is based on Tröger's base, a structure which has previously been employed to study host-guest chemistry and to quantify intermolecular interactions.[24–30] The model system was studied by a number of NMR methods, affording both *quantitative* (association constants and binding energies) and *qualitative* (conformation of the free and bound ligands) data for the binding of the different ligands to the receptor. The experimental data was then used to compare and evaluate a number of molecular mechanics (MM)[31] and dispersion-corrected density functional theory (DFT)[31] methods.

Results and Discussion

Description of the model system

Receptor **1** consists of a Tröger's base motif with 18-crown-6 moieties fused to each end of the aromatic cavity, and is synthesized in one step by the condensation of commercially

[a] A. Lidskog, Dr. S. Dawaigher, Dr. C. Solano Arribas, Dr. A. Ryberg, Dr. J. Jensen, Dr. K. E. Bergquist, Dr. A. Sundin, Prof. Dr. K. Wärnmark
Centre for Analysis and Synthesis, Department of Chemistry
Lund University
P. O Box 124, S-221 00 Lund (Sweden)
E-mail: kenneth.warnmark@chem.lu.se

[b] Prof. Dr. P.-O. Norrby
Data Science & Modelling, Pharmaceutical Sciences, R&D
AstraZeneca Gothenburg
Gothenburg (Sweden)
E-mail: per-ola.norrby@astrazeneca.com

Supporting information for this article is available on the WWW under https://doi.org/10.1002/chem.202100890

available 4-aminobenzo-18-crown-6 and formaldehyde in the presence of HCl in ethanol (Scheme 1a).[26] The C_2-symmetric V-shaped Tröger's base affords a well-defined hydrophobic cavity,[24] while crown-ethers are known to complex efficiently with primary ammonium ions.[32] We have previously reported on the interaction between receptor **1** and unsubstituted primary bisammonium chlorides.[26] The strongest interaction (highest association constant $K_{1\cdot x}$) was found for heptane-1,7-diyl bis(ammonium chloride), where the two ammonium groups are separated by seven carbon atoms (**2** in Scheme 1b). In addition, the study also found that the preferred conformation of bisammonium salt **2** is an all-*anti* conformation with the central methylene group (H-4) pointing towards the cavity of receptor **1** (Scheme 1b).[26]

As the intended use of the model system was to model the interactions between non-polar side chains of peptides and the aromatic cavity of a protein, a number of heptane-1,7-diyl bisammonium salts with different substituents in the 4-position were selected as ligands (Scheme 1b). The substituents were chosen to mimic different non-polar side chains of amino acids, as well as non-natural ligands. Unsubstituted ligand **2** was included to be used as a reference compound. The synthesis of receptor **1** and ligands **2–6** is described in the Supporting Information.

If the heptane backbone of the ligands were to have the same conformation within the series of ligands, determining the ΔG^0 value for the interaction between receptor **1** and each ligand **3–6** and subtracting with the ΔG^0 value of the unsubstituted ligand **2** would result in $\Delta\Delta G^0$ values that represent how strong the interaction of a specific "free" substituent would be with a "free" aromatic cavity of **1**, since the interactions common for all the heptane backbones would be cancelled out. However, the conception of a "uniform" conformation of the ligand backbone is as expected difficult to realize, especially in a system where there is such a large degree of conformational freedom in the backbone of the ligands (see below). On the other hand, an aliphatic backbone is a better biological model than a less flexible one. The most correct conceptual model in our case is that the $\Delta\Delta G^0$ values represent the standard free binding energy between the substituted ligand (**3**-**6**) and the aromatic cavity of receptor **1** in relation to the unsubstituted ligand **2**. Thus, the obtained $\Delta\Delta G^0$ values involve the binding energy between the substituent and the receptor, the rearrangement energy of the ligand backbone to fit to the receptor cavity, and the solvophobic interaction[33] of each ligand **3–6** in relation to ligand **2.**

Experimental estimation of absolute and relative association constants

Changes in the free energy of association for each of the bisammonium ligands **2–6** to receptor **1** can be determined via the estimation of the corresponding association constants ($K_{1\cdot x}$). NMR titration methodology is widely used to observe and quantify association processes between hosts and guests by estimating the association constants for the resulting complexes.[34–38] For an association process between a host and a guest in fast exchange on the NMR time scale, the observed chemical shift of a particular proton resonance in the guest is the weighted average of the particular proton resonance in the free guest and in the host-guest complex.[34,36] Initial ^{1}H NMR titrations of receptor **1** and unsubstituted ligand **2** showed that all proton resonances were observed as average chemical shifts

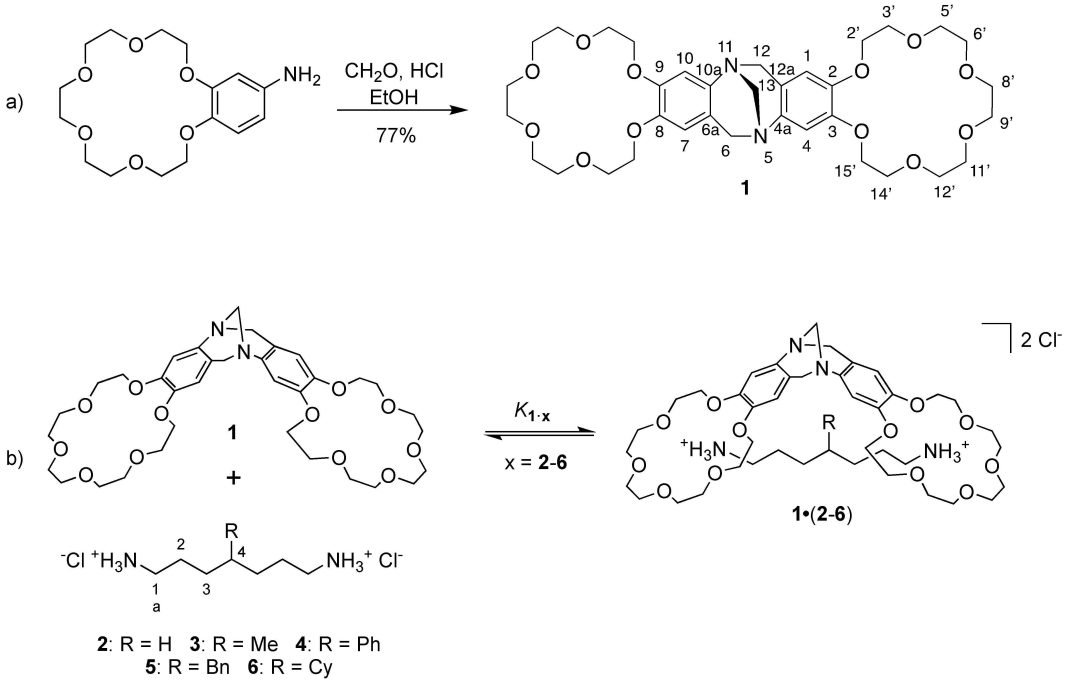

Scheme 1. a) Synthesis of bis(18-crown-6) Tröger's base receptor **1**.[26] b) Binding of ligands **2–6** to receptor **1**.

which depended on both the relative amount of **1** versus **2** and the total concentration.[26] This allowed for the use of NMR titration methodology to estimate association constants between the receptor and each of the bisammonium ligands.

As for the experimental conditions, the desire to emulate the conditions in a biological system and perform the experiments in water was offset by the limited solubility of the receptor. As a compromise, a 1:1 mixture of methanol and chloroform was used, where the methanol enables hydrogen bonding and solvophobic interactions similar to what would be present in a living cell while the chloroform solubilizes the receptor.

Binding stoichiometry

Before the association constants were estimated, the stoichiometry of the binding between receptor **1** and the bisammonium ligands (**2–6**) was determined. This was achieved by constructing a Job plot[39,40] using chemical shift data from ^{1}H NMR titrations between receptor **1** and ligand **3** in $CDCl_3$/MeOH-d_4 (1:1). The so-obtained Job plot (Figure S53) showed a 1:1 binding stoichiometry and this ratio was assumed to be valid for all of the complexes between receptor **1** and ligands **2–6**. This assumption was further supported by ES-mass spectrometry of solutions containing equimolar amounts of receptor **1** and each of the ligands **2–6**, where peaks corresponding to the 1:1 complexes **1**·(**2–6**) could be identified (Table S1 and Figure S54–S58).

Direct NMR titrations with methylammonium chloride as competitor

Fitting a 1:1 binding model to the NMR binding data of ligand **2** and receptor **1** revealed that the association constant was too high to be estimated directly ($K_{1\cdot2} > 10^5$ M^{-1}).[26,34] Instead, the association constants were measured relative to a weaker complex. This was accomplished by performing the titrations of the bisammonium salts in competition with a monoammonium salt for which the association constants could be determined by direct measurements. Methyl ammonium chloride (**7**) was chosen as the competitor since it had previously been shown to bind much more weakly to receptor **1** than bisammonium ligand **2**.[26] In addition, compound **7** has only one easily identified proton resonance which imposes little interference with other resonances in the ^{1}H NMR spectra. The addition of a monoammonium chloride salt also allowed us to maintain a constant chloride concentration throughout the titrations, thus mitigating the changes in ionic strength in the solution during the experiment.[41] Further details regarding the procedure for the NMR titrations are given in the Supporting Information.

The estimation of the association constants between the receptor and the bisammonium salts is based on the assumption that the association between the ditopic receptor (R) and the bisammonium ligand (B) follows a 1:1 binding model and will lead to one complex, as illustrated in Equation (1). The formation of a single complex rather than an oligomeric chain with 1:1 stoichiometry is strongly supported by the results from the ES-mass spectrometry (see above).

$$R + B \rightleftharpoons RB \; K^{bis} = \frac{[RB]}{[R][B]} \tag{1}$$

However, since the titrations were performed in competition with a monoammonium salt (M), the equilibria expressed by Equations (2) and (3) are also operating and need to be considered.

$$R + M \rightleftharpoons RM \; K_1^{mono} = \frac{[RM]}{[R][M]} \tag{2}$$

$$RM + M \rightleftharpoons RM_2 \; K_2^{mono} = \frac{[RM_2]}{[RM][M]} \tag{3}$$

Taking into account the equations above, the total concentration of R, B and M are given by Equations (4)–(6):

$$[R]_{total} = [R] + [RM] + [RM_2] + [RB] \tag{4}$$

$$[B]_{total} = [B] + [RB] \tag{5}$$

$$[M]_{total} = [M] + [RM] + 2[RM_2] \tag{6}$$

The concentration of all species containing receptor R and/or monoammonium salt M can be obtained by insertion of Equations (1), (2) and (3) into Equation (4) and (6), resulting in Equations (7), (8), (9) and (10):

$$[R] = \frac{[R]_{total}}{1+K_1^{mono}[M](1+K_2^{mono}[M])+K^{bis}[B]} \tag{7}$$

$$[RM] = \frac{[R]_{total}-[R](1+K^{bis}[B])}{1+K_2^{mono}[M]} \tag{8}$$

$$[RM_2] = [R]_{total}-[R](1+K_1^{mono}[M]+K^{bis}[B]) \tag{9}$$

$$[M] = \frac{[M]_{total}}{1+K_1^{mono}[R] + 2K_1^{mono}K_2^{mono}[R][M]} \tag{10}$$

The concentration of the free bisammonium salt, [B], can be obtained by insertion of Equation (1) into Equation (5), leading to Equation (11):

$$[B] = \frac{[B]_{total}}{1+K^{bis}[R]} \tag{11}$$

The observed chemical shift δ^m_{obs} for a given proton resonance m in any species containing monoammonium salt M is given by Eqaution (12):

$$\delta^m_{obs} = x_M\delta^m_M + x_{RM}\delta^m_{RM} + x_{RM_2}\delta^m_{RM_2} \tag{12}$$

where $x_M = [M]/[M]_{total}$, $x_{RM} = [RM]/[R]_{total}$ and $x_{RM2} = [RM_2]/[R]_{total}$.

The observed chemical shift δ^{b}_{obs} for a given resonance b in any species containing bisammonium salt B is given by Equation (13):

$$\delta^{b}_{obs} = x_B\delta^{b}_{B} + x_{RB}\delta^{b}_{RB} \quad (13)$$

where $x_B = [B]/[B]_{total}$ and $x_{RB} = [RB]/[R]_{total}$.

The association constants for each of the complexes **1**·(**2**–**6**) were determined using the equations above and an iterative process, which is further described in the Supporting Information. The estimation was based on the chemical shifts of the α-proton resonances of the ligands. Rewardingly, the change in the chemical shift was relatively sharp and responded well to the changes in the ratio between the receptor and the ligand (Figure S59 and S60).

The estimated association constants are shown in Table 1, together with the relative association constants in relation to the unsubstituted ligand **2**. The table also contains the range of the probability of binding (*p*) for the titrations, which should range between 0.2 and 0.8 in order to obtain an accurate value of $K_{1\cdot x}$.[34]

The quality of the fit of the model is demonstrated by the good correlation between the calculated and observed chemical shifts (Figure 1). The good fit further corroborates the 1:1 binding model [Eq. (1)] suggested by the Job plot and the ESI-MS experiments. The good fit also supports the assumption that any association of the monoammonium salt competitor to the receptor in the presence of bisammonium salt can be neglected, in accordance with earlier analysis.[26]

Table 1. Estimated absolute and relative association constants, as well as probability of binding values, for the association of ligands **2**–**6** to receptor **1**, obtained from direct NMR titrations in $CDCl_3$:MeOH-d_4 (1:1) with monoammonium salt **7** as competitor.

Ligand (**x**)	**2**	**3**	**4**	**5**	**6**
$\log K^{bis}_{1\cdot x}$	6.96	7.20	7.68	6.83	6.41
$K^{bis}_{1\cdot x}/K^{bis}_{1\cdot 2}$	1	1.74	5.25	0.74	0.28
Ranking[a]	*3*	*2*	*1*	*4*	*5*
Probability of binding (*p*)	0.42–0.95	0.51–0.92	0.68–0.96	0.37–0.94	0.22–0.81

[a] Ranking of the ligands with respect to how well they bind to the receptor.

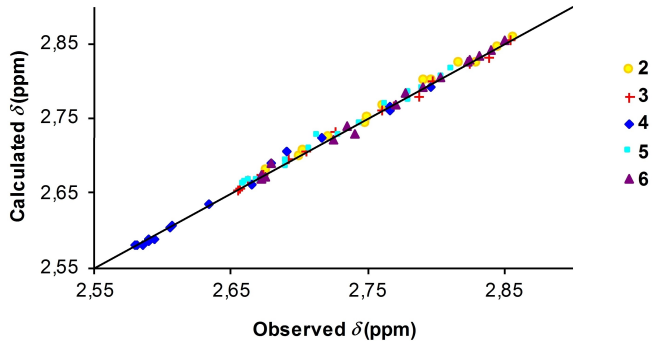

Figure 1. The correlation between observed and calculated chemical shifts for the α-protons of the different bisammonium salts (**2**–**6**) from NMR titrations with receptor **1** and monoammonium salt **7**. The NMR titrations were performed in $CDCl_3$/MeOH-d_4 (1:1) at $[Cl^-] = 74$ mM.

Pair-wise competitive NMR titrations

As can be seen in Table 1, the difference in the estimated association constants for complexes **1**·(**2**–**6**) is relatively small. When also taking into account the estimated uncertainties, the relative discrimination of bisammonium ligands **2**–**6** by receptor **1** becomes difficult to establish with high accuracy. In order to obtain more reliable information about the affinity of receptor **1** for each bisammonium ligand, pair-wise competitive NMR titrations were conducted, where each of the ligands **2**–**3** and **5**–**6** had to compete for binding to receptor **1** with ligand **4**. The phenyl substituted ligand **4** was chosen as the common competitor in all experiments due to the low degree of overlap between its α-proton resonance and the resonances of the other ligands in the ^{1}H NMR spectra during the titrations. The titrations were conducted in the presence of monoammonium salt **7** to keep the conditions as similar as possible to the ones used in the previous estimation of the absolute association constants.

The ratio between the association constant of ligand **x** (**x** = **2**–**3** and **5**–**6**) and ligand **4** with receptor **1**, $K^{bis}_{1\cdot x}/K^{bis}_{1\cdot 4}$, can be expressed as Equation (14) (see Supporting Information for derivation).[42]

$$\left(\delta^{bx}_{obs} - \delta^{bx}_{x}\right)\left(\delta^{b4}_{1\cdot 4} - \delta^{b4}_{obs}\right) = \frac{K^{bis}_{1\cdot x}}{K^{bis}_{1\cdot 4}}\left(\delta^{bx}_{1\cdot x} - \delta^{bx}_{obs}\right)\left(\delta^{b4}_{obs} - \delta^{b4}_{4}\right) \quad (14)$$

where b**x** and b**4** stand for a given proton resonance in ligand **x** and **4**, respectively. Same as for the direct titrations, the changes in the chemical shifts of the α-proton resonances were followed. Due to the large difference in the association constants between the bisammonium ligands and monoammonium salt **7**, the monoammonium salt is not expected to compete with the bisammonium ligands in the binding to receptor **1**.[26] Hence, Equation (14) can be considered a valid description of the present titration system.

The model as represented by Equation (14) was fitted to the experimental data using linear regression (Figure 2). The relative association constants ($K^{bis}_{1\cdot x}/K^{bis}_{1\cdot 4}$) are given by the slopes of the respective lines. Rewardingly, the high quality of the fit suggests that additional weaker associations (i.e. between receptor **1** and the monoammonium salt **7**) or slight deprotonation of the ammonium salts at low concentrations do not affect the value of the relative association constants.

The so-obtained relative association constants are given in Table 2. The relative association constants were also recalculated relative to **1**·**2**, as the unsubstituted ligand **2** was intended to be used as a reference compound. The good agreement between the relative association constants obtained by direct titrations (Table 1) and pair-wise competitive titrations (Table 2) show that despite the fact that the probability of

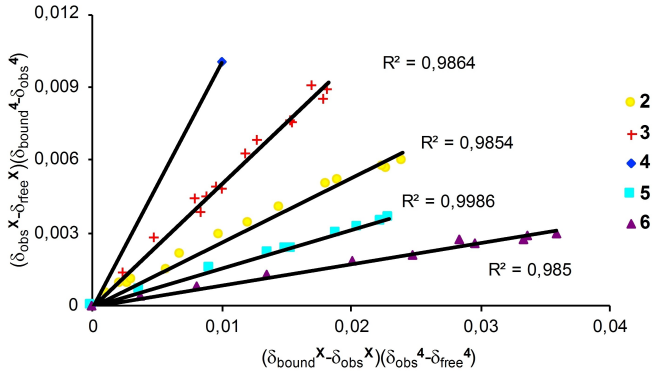

Figure 2. Fitting of the model represented by Equation (14) to experimental data for the estimation of the relative association constants of **1**·**2**, **1**·**3**, **1**·**4**, **1**·**5**, **1**·**6**, respectively, estimated relative to **1**·**4**. The relative association constant $K_{1\cdot x}/K_{1\cdot 4}$ is given by the slope of each straight line. The NMR titrations were performed in $CDCl_3$:MeOH-d_4 (1:1) with $[Cl^-]=74$ mM.

Table 2. Estimated relative association constants for the association of each of the ligands **2**–**6** to receptor **1**, obtained from pair-wise competitive titrations in $CDCl_3$:MeOH-d_4 (1:1) using ligand **4** as the competitor.

Ligand (**x**)	**2**	**3**	**4**	**5**	**6**
$K^{bis}_{1\cdot x}/K^{bis}_{1\cdot 4}$	0.26	0.51	1	0.15	0.09
$K^{bis}_{1\cdot x}/K^{bis}_{1\cdot 2}$	1	1.96	3.85	0.58	0.35
Ranking[a]	*3*	*2*	*1*	*4*	*5*

[a] Ranking of the ligands with respect to how well they bind to the receptor.

binding (*p*) did not completely cover the recommended 0.2–0.8 range in all titrations[34] and that the difference between the association constants was small, reliable association constants could be obtained from the direct titrations using weakly binding monoammonium ligand **7** as the competitor. Both titration methods resulted in the same ranking of the ligands with respect to the binding to the receptor, with phenyl-substituted ligand **4** binding the strongest, followed by ligand **3** (methyl), **2** (unsubstituted), **5** (benzyl) and **6** (cyclohexyl).

Experimental estimation of binding energies

As one of the aims of this study was to evaluate various computational methods by benchmarking against experimentally determined values, the relative association constants were converted into $\Delta\Delta G^0$ values using Equation (15). The results are given in Table 3.

Table 3. Experimentally determined values of $\Delta\Delta G^0_{1\cdot x-1\cdot 2}$ (kJ mol^{-1}) at 25 °C for the association of ligands **2**–**6** to receptor **1** in $CDCl_3$:MeOH-d_4 (1:1).

Ligand (**x**)	**2**	**3**	**4**	**5**	**6**
$\Delta\Delta G^0_{1\cdot x-1\cdot 2}$	0	−1.67	−3.34	1.35	2.60
Ranking[a]	*3*	*2*	*1*	*4*	*5*

[a] Ranking of the ligands with respect to how well they bind to the receptor.

$$\Delta\Delta G^0_{1\cdot x-1\cdot 2} = \Delta G^0_{1\cdot x} - \Delta G^0_{1\cdot 2} = -RT\ln\frac{K^{bis}_{1\cdot x}}{K^{bis}_{1\cdot 2}} \quad (15)$$

Phenyl-substituted ligand **4** exhibits the strongest binding to receptor **1**, followed by methyl-substituted ligand **3**, unsubstituted ligand **2**, benzyl-substituted ligand **5** and cyclohexyl-substituted ligand **6**. Rewardingly, the estimated free energy of the interaction between the methyl group of **3** and the aromatic cavity of **1** (−1.67 kJ mol^{-1}) is comparable to values obtained for a similar CH-π interaction by Wilcox's torsion balance (−2.1 kJ mol^{-1} in $CDCl_3$ and −3.0 kJ mol^{-1} in D_2O).[30] Since Wilcox's torsion balance also employs a Tröger's base analogue as a functional model and has similar constraints as our system, it is a good method to validate against. The involvement of a CH-π interaction in complex **1**·**3** is also supported by the conformational studies (see below). The free energy of the interaction between the phenyl group of **4** and the aromatic cavity of **1** (−3.34 kJ mol^{-1}) is higher than the corresponding value obtained from Wilcox's torsion balance in $CDCl_3$ (−1.1 kJ mol^{-1}).[29] One explanation for this could be that the phenyl group of **4** interacts with both aromatic moieties of receptor **1** with both π-π and CH-π interactions, something which is possible according to the conformational analysis of complex **1**·**4** (see below). It should also be noted that the only available π-π interaction value for Wilcox's torsion balance is measured in $CDCl_3$ and it is possible that a value obtained in a more polar solvent (e.g. D_2O or MeOH-d_4) would have been higher and more comparable to our estimated value, since our values are obtained using $CDCl_3$/MeOH-d_4 (1:1) as solvent.

Computational calculation of binding energies

The generated experimental relative binding energies were used to evaluate a number of MM and DFT methods with respect to binding energies.

Calculation of binding energies using molecular mechanics with different force fields

For each of the ligands **2**–**6** and the complexes **1**·(**2**–**6**), a set of conformations was generated by performing conformational searches (see Supporting Information). The sets of conformations were then minimized using three different force fields (MM3*,[43,44] MMFFs[45] and OPLS3e[46,47]). All MM calculations were performed using MacroModel,[48,49] so the choice of force field was limited to those available in that software package. The MM3* and MMFFs force fields were selected because they were developed for small molecules,[44,45] and have previously been compared favorably to other force fields.[50] The OPLS3e force field was included as it is the latest version of Schrödinger's own OPLS3 force field.[46] The minimizations were performed using both a chloroform solvent model and a water one, in order to compare with the experimental conditions ($CDCl_3$/MeOH-d_4 (1:1)). This resulted in two sets of conforma-

tions and corresponding E_0 values for each ligand/complex and force field, one in chloroform and one in water (see Supporting Information).

The change in energy when a ligand **x** binds to receptor **1** can be calculated by subtracting the energies of the free receptor and ligand from the energy of the complex, as shown in Equation (16):

$$\Delta E^{\mathrm{MM,solvent}}_{0,\mathbf{1}\cdot\mathbf{x}} = E^{\mathrm{MM,solvent}}_{0,\mathbf{1}\cdot\mathbf{x}} - E^{\mathrm{MM,solvent}}_{0,\mathbf{1}} - E^{\mathrm{MM,solvent}}_{0,\mathbf{x}} \quad (16)$$

where E_0 corresponds to the calculated potential energy, the subscript 0 denotes the lowest energy conformation and "solvent" denotes the solvent model used.

The change in binding energy relative to complex **1·2** can then be calculated according to Equation (17), where the E_0 values for free receptor **1** are cancelled out. This way of calculating the relative change in binding energy makes the comparison isodesmic and is expected to cancel out some of the systematic errors arising from for example neglected entropy terms, as well as deficiencies in the force fields.

$$\begin{aligned}\Delta\Delta E^{\mathrm{MM,solvent}}_{0,\mathbf{1}\cdot\mathbf{x}-\mathbf{1}\cdot\mathbf{2}} &= \Delta E^{\mathrm{MM,solvent}}_{0,\mathbf{1}\cdot\mathbf{x}} - \Delta E^{\mathrm{MM,solvent}}_{0,\mathbf{1}\cdot\mathbf{2}} \\ &= E^{\mathrm{MM,solvent}}_{0,\mathbf{1}\cdot\mathbf{x}} - E^{\mathrm{MM,solvent}}_{0,\mathbf{x}} - E^{\mathrm{MM,solvent}}_{0,\mathbf{1}\cdot\mathbf{2}} + E^{\mathrm{MM,solvent}}_{0,\mathbf{2}}\end{aligned} \quad (17)$$

Since the calculated $\Delta\Delta E^{\mathrm{MM,solvent}}_{0,\mathbf{1}\cdot\mathbf{x}-\mathbf{1}\cdot\mathbf{2}}$ values do not contain any entropic terms, they do not represent free energies. Therefore, to allow for a better comparison with the experimental $\Delta\Delta G^{0}_{\mathbf{1}\cdot\mathbf{x}-\mathbf{1}\cdot\mathbf{2}}$ values, a Boltzmann correction was introduced, which sums up the energy contributions of all conformers within 21 kJ mol^{-1} of the lowest energy conformation for each free ligand (**2**–**6**) and complex (**1**·(**2**–**6**)) [Eq. (18)].

$$E_{\mathrm{Boltzmann}} = E_0 - RT\ln\sum\nolimits_i e^{(E_0-E_i)/RT} \quad (18)$$

The Boltzmann-corrected change in binding energy relative to complex **1·2**, $\Delta\Delta E^{\mathrm{MM,solvent}}_{\mathrm{Boltzmann},\mathbf{1}\cdot\mathbf{x}-\mathbf{1}\cdot\mathbf{2}}$, could then be calculated according to Equation (19):

$$\begin{aligned}\Delta\Delta E^{\mathrm{MM,solvent}}_{\mathrm{Boltzmann},\mathbf{1}\cdot\mathbf{x}-\mathbf{1}\cdot\mathbf{2}} &= \Delta E^{\mathrm{MM,solvent}}_{\mathrm{Boltzmann},\mathbf{1}\cdot\mathbf{x}} - \Delta E^{\mathrm{MM,solvent}}_{\mathrm{Boltzmann},\mathbf{1}\cdot\mathbf{2}} \\ &= E^{\mathrm{MM,solvent}}_{\mathrm{Boltzmann},\mathbf{1}\cdot\mathbf{x}} - E^{\mathrm{MM,solvent}}_{\mathrm{Boltzmann},\mathbf{x}} - E^{\mathrm{MM,solvent}}_{\mathrm{Boltzmann},\mathbf{1}\cdot\mathbf{2}} + E^{\mathrm{MM,solvent}}_{\mathrm{Boltzmann},\mathbf{2}}\end{aligned} \quad (19)$$

Table 4 shows the calculated relative binding energies obtained with each of the force fields (MM3*, MMFFs and OPLS3e), using either a chloroform or a water solvent model. Values are given both with ($\Delta\Delta E^{\mathrm{MM}}_{\mathrm{Boltzmann},\mathbf{1}\cdot\mathbf{x}-\mathbf{1}\cdot\mathbf{2}}$) and without $\left(\Delta\Delta E^{\mathrm{MM}}_{0,\mathbf{1}\cdot\mathbf{x}-\mathbf{1}\cdot\mathbf{2}}\right)$ the Boltzmann correction. Table 4 also contains the experimentally determined $\Delta\Delta G^{0}_{\mathbf{1}\cdot\mathbf{x}-\mathbf{1}\cdot\mathbf{2}}$ values against which the calculated values are compared, and also the ranking of the ligands with respect to their binding to the receptor.

Comparing the calculated $\Delta\Delta E^{\mathrm{MM}}_{\mathbf{1}\cdot\mathbf{x}-\mathbf{1}\cdot\mathbf{2}}$ values with the experimentally determined $\Delta\Delta G^{0}_{\mathbf{1}\cdot\mathbf{x}-\mathbf{1}\cdot\mathbf{2}}$ values (Table 4) shows that the calculations performed with the MM3* force field and a chloroform solvent model result in a fairly accurate estimation of the binding affinity of the different ligands (**2**–**6**) to receptor **1**, both in terms of absolute values and in terms of the ranking of the binding of the ligands to the receptor. Both with and without the Boltzmann correction, the MM3* force field with a chloroform solvent model predicts the exact same order of binding as was determined experimentally, with phenyl-substituted ligand **4** binding the strongest and cyclohexyl-substituted ligand **6** binding the weakest. Except for the cyclohexyl-substituted ligand, all of the calculated $\Delta\Delta E^{\mathrm{MM}}_{\mathbf{1}\cdot\mathbf{x}-\mathbf{1}\cdot\mathbf{2}}$ values are within 2 kJ mol^{-1} of the experimentally determined $\Delta\Delta G^{0}_{\mathbf{1}\cdot\mathbf{x}-\mathbf{1}\cdot\mathbf{2}}$ values. The cyclohexyl-substituted ligand (**6**) is a clear outlier, with calculated $\Delta\Delta E$ values of 21.51 kJ mol^{-1} and 18.97 kJ mol^{-1} with and without Boltzmann correction, respectively, compared to the experimentally found 2.60 kJ mol^{-1}.

Table 4. Calculated $\Delta\Delta E^{\mathrm{MM}}_{\mathbf{1}\cdot\mathbf{x}-\mathbf{1}\cdot\mathbf{2}}$ values (kJ mol^{-1}) obtained using molecular modelling with different force fields and solvent models. Values without[a] and with[b] Boltzmann corrections are reported.

Ligand (**x**)		**2**	**3**	**4**	**5**	**6**
Experimental		0	−1.67	−3.34	1.35	2.60
Ranking[c]		*3*	*2*	*1*	*4*	*5*
MM3*	$CHCl_3$[a]	0	−2.17	−5.16	1.23	21.51
Ranking[c]		*3*	*2*	*1*	*4*	*5*
	$CHCl_3$[b]	0	−2.25	−5.21	0.30	18.97
Ranking[c]		*3*	*2*	*1*	*4*	*5*
	Water[a]	0	−4.42	−6.45	−8.78	13.14
Ranking[c]		*4*	*3*	*2*	*1*	*5*
	Water[b]	0	−4.37	−6.72	−4.97	15.17
Ranking[c]		*4*	*3*	*1*	*2*	*5*
MMFFs	$CHCl_3$[a]	0	−4.18	−2.45	−9.49	9.89
Ranking[c]		*4*	*2*	*3*	*1*	*5*
	$CHCl_3$[b]	0	−3.52	−1.41	−7.09	8.74
Ranking[c]		*4*	*2*	*3*	*1*	*5*
	Water[a]	0	−5.94	−9.78	−14.23	6.80
Ranking[c]		*4*	*3*	*2*	*1*	*5*
	Water[b]	0	−4.73	−10.17	−12.21	7.04
Ranking[c]		*4*	*3*	*2*	*1*	*5*
OPLS3e	$CHCl_3$[a]	0	−3.06	1.63	−5.83	7.33
Ranking[c]		*3*	*2*	*4*	*1*	*5*
	$CHCl_3$[b]	0	−3.98	1.83	−5.53	7.52
Ranking[c]		*3*	*2*	*4*	*1*	*5*
	Water[a]	0	−5.62	−4.26	−13.90	25.71
Ranking[c]		*4*	*2*	*3*	*1*	*5*
	Water[b]	0	−6.05	−7.45	−12.13	25.73
Ranking[c]		*4*	*3*	*2*	*1*	*5*

[a] Values obtained using only the lowest energy conformation, $\left(\Delta\Delta E^{\mathrm{MM}}_{0,\mathbf{1}\cdot\mathbf{x}-\mathbf{1}\cdot\mathbf{2}}\right)$. [b] Values obtained using the lowest energy conformation corrected with a Boltzmann term, $\Delta\Delta E^{\mathrm{MM}}_{\mathrm{Boltzmann},\mathbf{1}\cdot\mathbf{x}-\mathbf{1}\cdot\mathbf{2}}$. [c] Ranking of the ligands with respect to how well they bind to the receptor.

Performing the MM3* calculations with a water solvent model results in overall less accurate values, most significantly for the benzyl-substituted ligand (**5**), which according to the calculations is estimated to bind more favorably to the receptor than what was found experimentally (Table 4). Without the Boltzmann correction, ligand **5** is ranked as the strongest binding ligand, with a $\Delta\Delta E_0$ value of −8.78 kJ mol^{-1}. This is in stark contrast to the experimental findings, where the benzyl-substituted ligand is the second weakest binding (1.35 kJ mol^{-1}). Applying the Boltzmann correction results in a more accurate $\Delta\Delta E_{\mathrm{Boltzmann}}$ value for ligand **5** (−4.97 kJ mol^{-1}) and a more

correct ranking of the binding of the ligands, with phenyl-substituted ligand **4** binding the strongest (same as what is found experimentally). Similar to what was observed with a chloroform solvent model, using a water solvent model also results in overestimated $\Delta\Delta E$ values for the cyclohexyl-substituted ligand (**6**) (13.14 kJ mol^{-1} and 15.17 kJ mol^{-1} with and without Boltzmann correction, respectively, compared to the experimentally found 2.60 kJ mol^{-1}), although this overestimation is smaller than what was obtained with the chloroform solvent model.

The MM calculations performed with the MMFFs force field give overall less accurate binding energies (Table 4). Calculations with both solvent models (chloroform and water) correctly predict the cyclohexyl-substituted ligand (**6**) as binding the weakest, but incorrectly identifies benzyl-substituted ligand **5** as binding the strongest. This is especially clear with a water solvent model, which gives a $\Delta\Delta E_0$ value of −14.23 kJ mol^{-1} for ligand **5** (−12.21 kJ mol^{-1} after Boltzmann correction), compared to the experimentally found 1.35 kJ mol^{-1}. Compared to MM3*, the MMFFs force field gives more accurate $\Delta\Delta E$ values for cyclohexyl-substituted ligand **6**, with values in the range of 6.80–9.89 kJ mol^{-1} (depending on solvent model and Boltzmann correction). While the values are still higher than the experimentally found $\Delta\Delta G^0$ value of 2.60 kJ mol^{-1}, they are significantly closer than the values obtained with MM3* (13.14–21.51 kJ mol^{-1}). Between the two solvent models, the $\Delta\Delta E$ values obtained with a chloroform solvent model are closer to the experimentally determined $\Delta\Delta G^0$ values, while the water solvent model gives a more correct ranking of the ligands. Application of the Boltzmann correction generally improves the $\Delta\Delta E$ values but does not change the ranking of the ligands with respect to their binding to the receptor compared to the uncorrected $\Delta\Delta E$ values.

The MM calculations performed with the OPLS3e force field result in $\Delta\Delta E^{MM}_{1\cdot x-1\cdot 2}$ values which deviate from the experimental $\Delta\Delta G^0_{1\cdot x-1\cdot 2}$ values to a varying degree (Table 4). As was observed for the MMFFs force field, the OPLS3e calculations correctly predict the cyclohexyl-substituted ligand (**6**) as binding the weakest to the receptor with either solvent model (chloroform or water), but incorrectly identifies benzyl-substituted ligand **5** as binding the strongest. In addition, the calculations performed with a chloroform model predict the phenyl-substituted ligand (**4**) as binding the second weakest, which is far from the experimental results where ligand **4** binds the strongest. The use of the water solvent model results in a ranking of the ligands more similar to what was found experimentally. In terms of absolute values, the chloroform solvent model affords calculated $\Delta\Delta E^{MM}_{1\cdot x-1\cdot 2}$values ranging from −5.83 to 7.33 kJ mol^{-1}, which is relatively close to the range of the experimental values (−3.34-2.60 kJ mol^{-1}). The use of the water solvent model instead results in several values which deviate significantly from what was found experimentally, including benzyl-substituted ligand **5** (−13.90 kJ mol^{-1}, compared to experimental 1.35 kJ mol^{-1}) and cyclohexyl-substituted ligand **6** (25.71 kJ mol^{-1}, compared to experimental 2.60 kJ mol^{-1}). For both solvent models, the use of the Boltzmann correction does not significantly improve the estimation of the binding energies.

In general, more accurate predictions of the strength of the binding of ligands **2–6** to receptor **1** are obtained with the chloroform solvent model than with the water solvent model. The initial idea was to make a linear combination of the values obtained with a chloroform solvent model and the values obtained with a water solvent model, in order to approximate the experimental conditions of $CDCl_3$/MeOH-d_4 (1 : 1). However, it appears that the water solvent model is too polar for this kind of approximation and the most accurate values are obtained by just using the energies calculated with a chloroform solvent model.

Another observation is the fact that the Boltzmann correction does not overall improve the accuracy of the calculated binding energies (Figure S61). In some cases, the use of the Boltzmann correction does result in slightly better values (e.g. MMFFs with a chloroform solvent model), while in other cases, the calculated binding energies become less accurate (e.g. OPLS3e with a water model). A possible explanation for this could be that the compared systems (free ligands and ligand-receptor complexes) have very similar distributions of conformations.

A qualitative analysis of the ability of the different force fields to predict the overall order of binding of the ligands to the receptor shows that all of the employed force fields predict the cyclohexyl-substituted ligand (**6**) to bind the weakest to the receptor, which is in accordance with the experimental findings. As for the strongest binding ligand, the MM3* force field identifies the phenyl-substituted ligand (**4**) as binding the strongest, while both MMFFs and OPLS3e instead find the benzyl-substituted ligand (**5**) to have the strongest binding to the receptor. Compared to the experimental results, where the phenyl-substituted ligand **4** is found to bind the strongest and benzyl-ligand **5** is found to bind second to weakest, this clearly indicates that the MM3* force field gives a more accurate prediction.

A quantitative analysis of the ability of the different force fields to predict the strength of the binding of the different ligands to the receptor could either be conducted by comparing the individual $\Delta\Delta E^{MM}_{1\cdot x-1\cdot 2}$ values with the corresponding experimentally determined $\Delta\Delta G^0_{1\cdot x-1\cdot 2}$ values, or by looking at the whole set of values. The latter case could be investigated by for example comparing the range of the calculated values with what was found experimentally, or by calculating the mean absolute error (MAE, Table S20). Due to the presence of single outliers, the MAE was deemed a less suitable measurement to evaluate the different force fields in our case. For the range of the calculated $\Delta\Delta E^{MM}_{1\cdot x-1\cdot 2}$ values, all of the force fields give a wider range of values than what was found experimentally ($\Delta\Delta G^0_{1\cdot x-1\cdot 2} = -3.34$–$2.60$ kJ mol^{-1}). The MM calculations performed with the OPLS3e force field and a chloroform solvent model give the most narrow range, with values ranging from −5.53 to 7.52 kJ mol^{-1}. As a comparison, the MM3* force field with a chloroform solvent model gives $\Delta\Delta E$ values ranging from −5.16 to 21.51 kJ mol^{-1}. While this is obviously a significantly wider range of values than what was found

experimenally, it is caused by a single outlier. The obtained $\Delta\Delta E^{MM}_{1\cdot x-1\cdot 2}$ values are very similar to the experimentally found $\Delta\Delta G^{0}_{1\cdot x-1\cdot 2}$ values for all ligands except for the cyclohexyl-substituted ligand (**6**). If this ligand is omitted, the values range between −5.16 and 1.23 kJ mol^{-1} (corresponding experimental range = −3.34–1.35 kJ mol^{-1}). In general, several of the force fields predict a significantly higher $\Delta\Delta E^{MM}_{1\cdot x-1\cdot 2}$ value for cyclohexyl-substituted ligand **6** than what was found experimentally (2.60 kJ mol^{-1}). For some of the force fields, this overestimation leads to clear outliers (e.g. MM3* with both solvent models and OPLS3e with a water solvent model). Similarly, with the exception of MM3* with a chloroform solvent model, all of the force fields predict benzyl-substituted ligand **5** to bind significantly stronger to the receptor (−4.97–−14.23 kJ mol^{-1}) than what was found experimentally (1.35 kJ mol^{-1}).

Calculation of binding energies using density functional theory

DFT calculations were performed using the M06-2X-D3[51] and ωB97X-D[52] functionals, with the 6–31G** basis set and a Poisson-Boltzmann (PBF) continuum solvation model[53] for chloroform. DFT calculations were performed on each of the free ligands **2–6** and the complexes **1**·(**2–6**), using the lowest energy conformations obtained from the MM calculations with the three different force fields (MM3*, MMFFs and OPLS3e) and fully optimized using a PBF model for chloroform solvent (see Supporting Information). The so-obtained lowest E^{DFT}_{0} values for each ligand and complex were then used to calculate relative binding energies according to Equation (20). The resulting $\Delta\Delta E^{MM}_{1\cdot x-1\cdot 2}$ values are presented in Table 5, which also includes the corresponding experimental values as well as the DFT values obtained in gas phase.

$$\Delta\Delta E^{DFT}_{0,1\cdot x-1\cdot 2} = E^{DFT}_{0,1\cdot x} - E^{DFT}_{0,x} - E^{DFT}_{0,1\cdot 2} + E^{DFT}_{0,2} \quad (20)$$

Overall, the DFT calculations result in predictions of the binding affinity of the different ligands (**2–6**) to receptor **1** which deviate significantly from what was determined experimentally, both in terms of absolute values and in terms of the ranking of the binding of the ligands to the receptor (Table 5). The predicted binding affinities are also significantly less accurate than what was obtained from MM calculations (Figure 3).

Quantitatively, the DFT calculations performed with the M06-2X-D3 functional results in slightly more accurate relative binding energies than calculations performed with the ωB97X-D functional. In addition, the relative binding energies calculated in gas phase are significantly more accurate than the relative binding energies calculated with a PBF chloroform model. The most drastic difference is seen for benzyl-substituted ligand **5**, where the $\Delta\Delta E^{DFT}$ values calculated with a PBF

Table 5. Calculated $\Delta\Delta E^{DFT}_{1\cdot x-1\cdot 2}$ values (kJ mol^{-1}) obtained from DFT calculations.[a]

Ligand (**x**)		**2**	**3**	**4**	**5**	**6**
Experimental		0	−1.67	−3.34	1.35	2.60
Ranking[b]		*3*	*2*	*1*	*4*	*5*
M06-2X-D3	$CHCl_3$[c]	0	−9.55	−18.01	−38.59	−28.17
Ranking[b]		*5*	*4*	*3*	*1*	*2*
	Gas phase	0	−8.77	−0.53	6.42	−25.66
Ranking[b]		*4*	*2*	*3*	*5*	*1*
ωB97X-D	$CHCl_3$[c]	0	−11.42	−20.78	−46.96	−31.81
Ranking[b]		*5*	*4*	*3*	*1*	*2*
	Gas phase	0	−9.92	−15.45	−1.97	−23.75
Ranking[b]		*5*	*3*	*2*	*4*	*1*

[a] All DFT calculations were performed with the 6–31G** basis set. [b] Ranking of the ligands with respect to how well they bind to the receptor. [c] Calculated with a PBF chloroform solvation model.

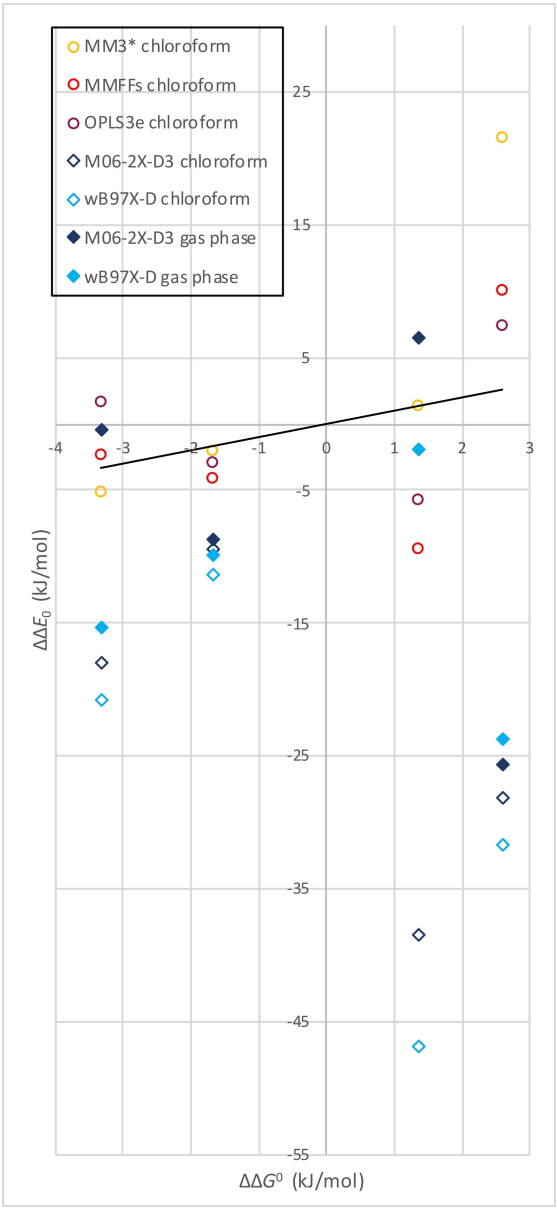

Figure 3. Comparison of calculated $\Delta\Delta E_0$ values obtained from MM (circles) and DFT calculations (diamonds) with experimentally determined $\Delta\Delta G^0$ values. The black line marks the diagonal.

chloroform solvent model are 45 kJ mol^{-1} lower than those calculated in gas phase, with the values calculated in gas phase being much more comparable to the experimental value (Table 5 and Figure 3).

Qualitatively, neither of the functionals (M06-2X-D3 or ωB97X-D) manage to predict the overall order of binding of the ligands to the receptor. The DFT calculations predict either the cyclohexyl-substituted ligand (**6**) or the benzyl-substituted ligand (**5**) to bind the strongest to the receptor, which in stark contrast to the experimental findings where ligand **6** binds the weakest and ligand **5** the second weakest.

Conformational analysis of the receptor-ligand complexes

In addition to evaluating the different computational methods in terms of their ability to predict the binding affinities of the different ligands (**2**–**6**) to the receptor **1**, efforts were also made to evaluate ability of the different force field methods to predict the conformation of the ligand, both in solution and when bound to the receptor. To this end, NMR spectroscopy data were used to suggest time-averaged conformations of the free ligands and the receptor-ligand complexes, which were then compared to energy-minimized structures obtained from MM calculations. The analysis was made using the lowest energy conformations obtained from MM calculations with the three force fields (MM3*, MMFFs and OPLS3e) and a chloroform solvent model, since those calculations afforded the most accurate $\Delta\Delta E$ values (see above). In addition, molecular dynamics (MD) simulations were conducted for each of the free ligands and receptor-ligand complexes, using the OPLS3e force field and a methanol solvent model (see Supporting Information).

The experimental information was obtained from a combination of the ^{1}H NMR titration data and NOESY and ROESY spectra. All NMR spectra and assignments are presented in the Supporting Information, as well as the conformational analysis of each of the free ligands **2**–**6**.

Conformation of complex 1·2

When going from free to bound to receptor **1**, the resonance of the central methylene protons (H-4) of ligand **2** is displaced dramatically upfield by 1.03 ppm (Figure S38). In addition, the proton resonances of H-1, H-2 and H-3 exhibit upfield shifts of 0.23, 0.70 and 0.53 ppm, respectively. This suggests that **2** is situated in the aromatic cavity of **1**, as previously concluded.[26] The sizes of the upfield shifts of H-1, H-2, H-3, and H-4 indicate that the ligand adopts an all-*anti* conformation on a time-average, where H-2 and H-4 are pointing towards the aromatic cavity and are thus more shielded. Although the H-4 protons are further away from the aromatic cavity than the H-2 protons, they experience the presence of two aromatic rings due to the V-shape of the cavity, which could explain the larger upfield shift. In the ROESY spectrum of complex **1·2** (Figure S40), cross peaks can be observed between H-1 and H-2, between H-1 and H-3, between H-2 and H-3, and between H-3 and H-4, indicating that they are within 3.5 Å of each other,[54] as expected for an all-*anti* conformation of the heptane chain of **2** in complex **1·2**. A cross peak between H-1 of ligand **2** and the crown-ether moieties of receptor **1** also supports that the ligand is complexed to the receptor.

It should be noted that for a qualitative conformational analysis, more emphasis should be placed on the change in chemical shift upon association of the ligand to the receptor, than on the NOESY/ROESY data, since the observed chemical shift of a proton resonance is directly proportional to the amount of each of different species (conformations) present in the system, while the nuclear/rotating-frame Overhauser effect (NOE/ROE) involves a r^{-6} distance term, meaning that conformations where the protons in questions are closer together will be given more weight than conformations where they are further apart, regardless of which conformation is more populated.[54] That being said, in this case, both the observed change in chemical shifts and the ROESY spectrum support an all-*anti* conformation of ligand **2** when bound to receptor **1**.

The energy-minimized conformations of complex **1·2** obtained from MM calculations with a chloroform solvent model and the three different force fields all suggest all-*anti* conformations of ligand **2**, with N–N distances varying between 9.85 and 10.11 Å (Figure 4). To corroborate the all-*anti* conformation, an MD simulation of complex **1·2** was performed with the OPLS3e force field and a methanol solvent model. The simulation shows an extended heptane chain of ligand **2**, with the N–N distance varying between 9 and 10 Å during the 200 ns simulation (Figure S81–82).

In conclusion, MM calculations with all three force fields and the chloroform solvent model are in agreement with the experimental observation of an all-*anti* heptane chain of complex **1·2**, with H-2 and H-4 oriented towards the aromatic cavity.

Conformation of complex 1·3

When going from free to bound to receptor **1**, the resonances of the methyl protons (H-5) and H-4 of ligand **3** are shifted drastically upfield by 1.07 and 0.99 ppm, respectively (Figure S41). The magnitude of the displacement indicates that both the methyl group and the H-4 proton are residing in or close to the aromatic cavity on a time-average. This is further supported by the ROESY spectrum of **1·3** (Figure S43), which shows cross peaks between the methyl protons of the ligand (H-5) and both H-1(H-7) and H-6$_{endo}$(H-12$_{endo}$) of the receptor. The larger upfield displacement of H-2 (0.66 ppm) compared to H-1 and H-3 (0.22 and 0.49 ppm, respectively) is consistent with an all-*anti* conformation of the heptane backbone of ligand **3**. This is further supported by the ROESY spectrum, which shows an intense cross peak between H-1 and H-2 of the ligand, and a weaker cross peak between H-1 and H-3.

The energy-minimized conformations of complex **1·3** obtained from MM calculations using the chloroform solvent model and the three different force fields show all-*anti*

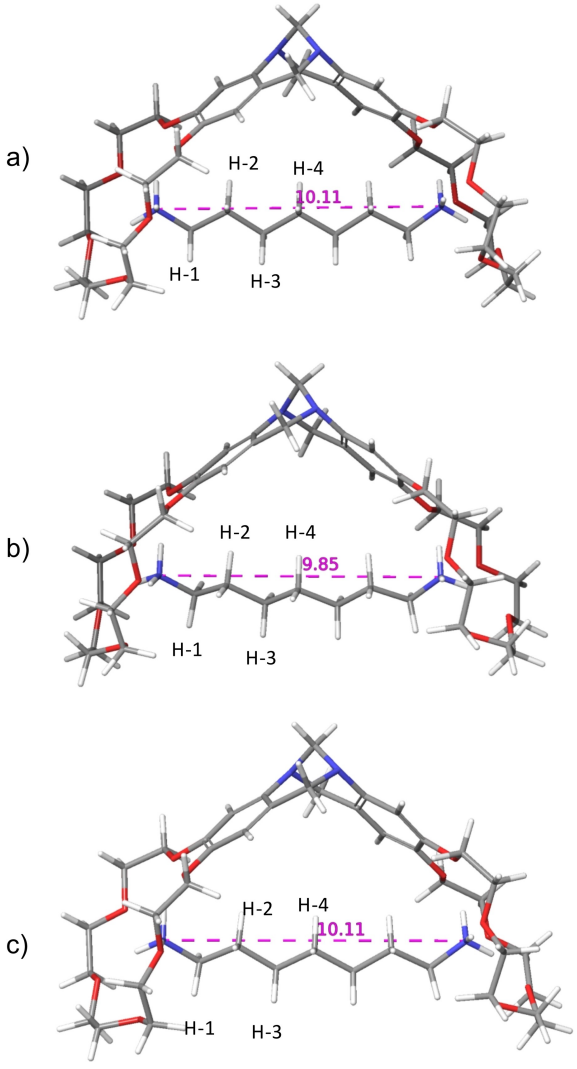

Figure 4. The lowest energy conformation of ligand **2** bound to receptor **1** from MM calculations performed with a chloroform solvent model. Force field: a) MM3* (N–N distance = 10.11 Å), b) MMFFs (N–N distance = 9.85 Å), c) OPLS3e (N–N distance = 10.11 Å).

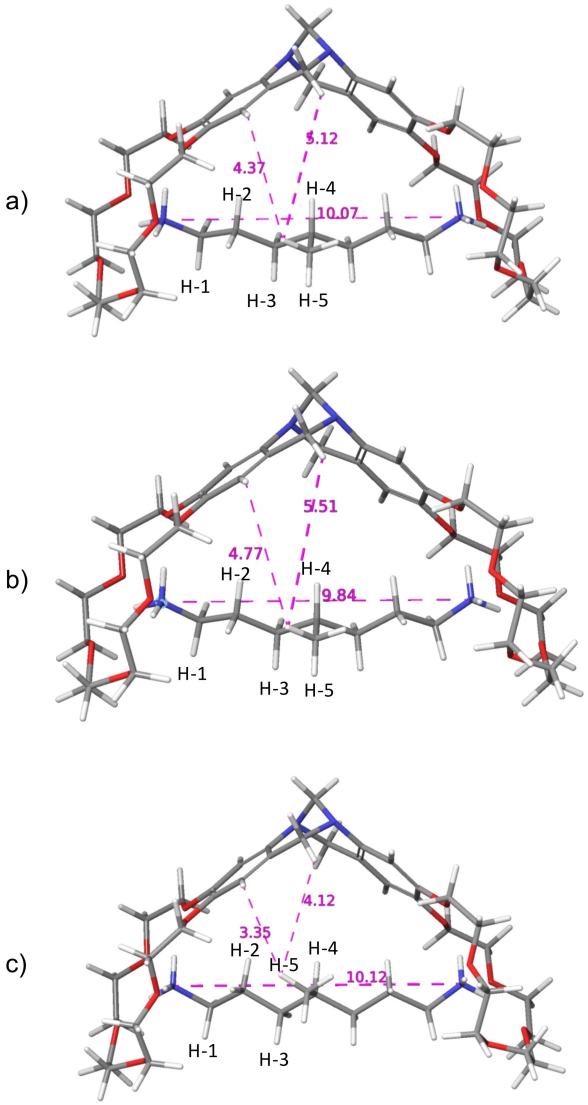

Figure 5. The lowest energy conformation of ligand **3** bound to receptor **1** from MM calculations performed with a chloroform solvent model. Force field: a) MM3* (N–N distance = 10.07 Å, $H5_{lig}$-$H6_{endo,rec}$ = 5.12 Å, $H5_{lig}$-$H1_{rec}$ = 4.37 Å), b) MMFFs (N–N distance = 9.84 Å, $H5_{lig}$-$H6_{endo,rec}$ = 5.51 Å, $H5_{lig}$-$H1_{rec}$ = 4.77 Å), c) OPLS3e (N–N distance = 10.12 Å, $H5_{lig}$-$H6_{endo,rec}$ = 4.12 Å, $H5_{lig}$-$H1_{rec}$ = 3.35 Å).

conformations of the backbone of ligand **3**, with N–N distances varying between 9.84 and 10.12 Å (Figure 5). The lowest energy conformations obtained with the MM3* and MMFFs force fields have the methyl group oriented somewhat out and away from the aromatic cavity of the receptor (Figure 5a,b). The conformation obtained with the OPLS3e force field show the methyl group more oriented towards the aromatic cavity (Figure 5c). The MD simulation of complex **1·3** performed with the OPLS3e force field and a methanol solvent model shows a mostly extended heptane chain, with the methyl substituent oriented towards the aromatic cavity of the receptor (Figure S83–84), supporting the results from the MM calculations using the OPLS3e force field.

In conclusion, MM calculations with all three force fields are in agreement with the experimental observation of an all-*anti* heptane chain of complex **1·3**. The orientation of the methyl group is most correctly predicted by the OPLS3e force field, which places it pointing towards the aromatic cavity of the receptor, as is suggested by the NMR data.

Conformation of complex 1·4

The NMR data suggest that the phenyl substituent of ligand **4** resides, at least partially, inside the aromatic cavity of receptor **1**. The most significant evidence for this is the upfield displacement of the resonances of the *ortho*-protons of the phenyl substituent (H-6) and H-4 of ligand **4**, which are shifted 0.75 and 1.26 ppm upfield, respectively (Figure S44). In addition, the broadening of the resonance of H-1(H-7) of the receptor indicates that it is interacting strongly with the phenyl

substituent of ligand **4**. The ROESY spectrum of **1**·**4** (Figure S46) provides further support for a conformation where the phenyl substituent of **4** is in close contact with the aromatic cavity of receptor **1**, with cross peaks between the *ortho*- and *meta*-protons (H-6 and H-7) of the phenyl substituent of ligand **4** and the H-6_{endo}(H-12_{endo}) protons of the receptor. The larger upfield displacement of H-2 (0.71 ppm) compared to H-1 and H-3 (0.30 and 0.39 ppm, respectively) is consistent with an all-*anti* conformation of the heptane backbone of ligand **4**. This is further supported by the ROESY spectrum, which shows cross peaks between H-1 and H-2, and between H-1 and H-3, similar to what was observed for complex **1**·**2**.

The energy-minimized conformations of complex **1**·**4** obtained from MM calculations using a chloroform solvent model and the MM3* and OPLS3e force fields show an all-*anti* conformation of the heptane chain of **4**, with N–N distances of 10.12 and 10.13 Å, respectively (Figure 6a,c). The lowest energy conformation obtained with the MMFFs force field includes one *gauche* interaction between C-2 and C-3 in the heptane chain, resulting in a shorter N–N distance of 9.59 Å (Figure 6b). For all three force fields, the phenyl substituent is oriented partly inside the aromatic cavity. The MD simulation of complex **1**·**4** performed with the OPLS3e force field and a methanol solvent model suggests a relatively rigid receptor-ligand complex. Over the 200 ns simulation, the N–N distance remains close to 10 Å, indicating an all-*anti* heptane backbone, while the phenyl substituent stays oriented towards the aromatic cavity (Figure S85–86), supporting the results from the MM calculations.

In conclusion, MM calculations performed with the MM3* and OPLS3e force fields are in agreement with the experimental observation of an all-*anti* heptane chain of complex **1**·**4**. All three force fields also place the phenyl group partly inside the aromatic cavity of the receptor, which is consistent with the NMR data.

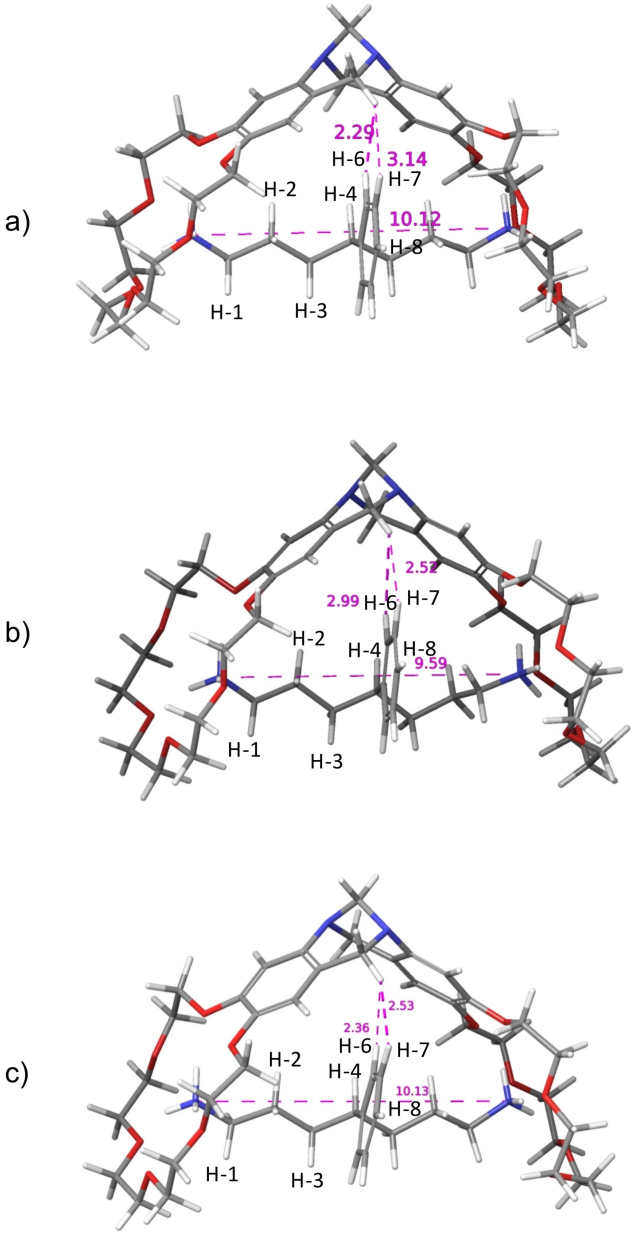

Figure 6. The lowest energy conformation of ligand **4** bound to receptor **1** from MM calculations performed with a chloroform solvent model. Force field: a) MM3* (N–N distance = 10.12 Å, $H6_{lig}$-$H6_{endo,rec}$ = 2.29 Å, $H7_{lig}$-$H6_{endo,rec}$ = 3.14 Å), b) MMFFs (N–N distance = 9.59 Å, $H6_{lig}$-$H6_{endo,rec}$ = 2.99 Å, $H7_{lig}$-$H6_{endo,rec}$ = 2.52 Å), c) OPLS3e (N–N distance = 10.13 Å, $H6_{lig}$-$H6_{endo,rec}$ = 2.36 Å, $H7_{lig}$-$H6_{endo,rec}$ = 2.53 Å).

Conformation of complex 1·5

When going from free to bound to receptor **1**, the resonance of the central methylene proton (H-4) of ligand **5** is displaced upfield by 0.85 ppm (Figure S47). In addition, the proton resonances of H-1, H-2 and H-3 exhibit upfield shifts of 0.19, 0.68 and 0.50 ppm, respectively. This suggests an all-*anti* conformation of the heptane backbone, with H-2 and H-4 oriented towards the aromatic cavity of receptor **1**. The ROESY spectrum (Figure S49) also show cross peaks between H-1 and H-2, and H-1 and H-3, which is consistent with an all-*anti* conformation of the heptane chain of ligand **5**, similar to what was seen for complex **1**·**2**. Based on the relatively smaller upfield displacement of H-4 compared to in complexes **1**·**3** and **1**·**4**, it can be assumed that H-4 of ligand **5** is not situated as deep inside the aromatic cavity of **1**.

Regarding the position of the benzyl substituent of ligand **5**, the relatively small upfield displacement of the methylene protons (H-5) and the *ortho*-protons (H-7) by 0.40 and 0.12 ppm, respectively, indicates that part of the benzyl substituent, mainly the methylene group, is situated inside or close to the aromatic cavity of receptor **1**, although to a lesser extent than the methyl group of **1**·**3** or the phenyl group of **1**·**4**. The minor displacement of the *ortho*-protons of **5** (H-7), combined with the slight downfield displacement of the *meta*- and *para*-protons (H-8 and H-9, ~0.12 ppm), indicate that the benzyl group is actually pointing away from the aromatic cavity of receptor **1**, with the *ortho*-protons being closest to the cavity. This is further supported by the ROESY spectrum (Figure S49), which shows cross peaks between the *ortho*-protons (H-7) of the ligand and H-1 and H-6_{endo} of the receptor. The ROESY

spectrum also exhibits cross peaks between both the *ortho*- and *meta*-protons of the benzyl substituent of the ligand (H-7 and H-8) and the crown ether moieties of the receptor, which indicates a rather dynamic system where the benzyl substituent has a lot of flexibility.

The energy-minimized conformation of complex **1·5** obtained from MM calculations using a chloroform solvent model and the MM3* force field shows an all-*anti* conformation of the heptane chain of **4**, with an N–N distance of 10.10 Å (Figure 7a), while the conformations obtained with the MMFFs and OPLS3e force fields contain two *gauche* interactions each (N–N distance 9.11 and 9.47 Å, respectively, Figure 7b,c). The three different

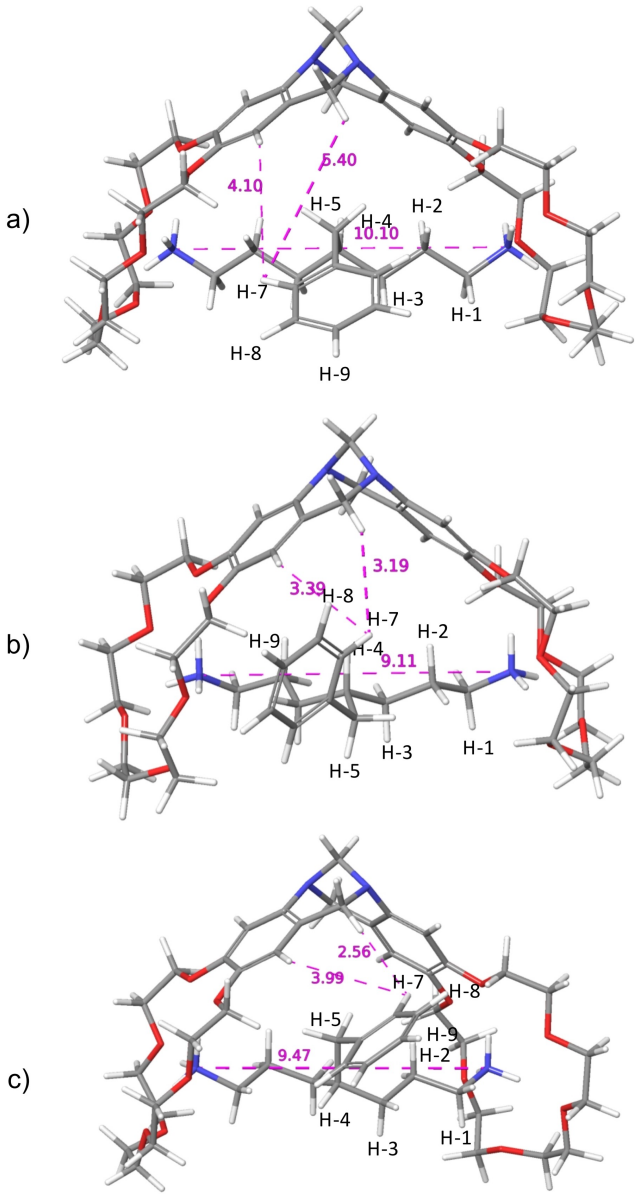

Figure 7. The lowest energy conformation of ligand **5** bound to receptor **1** from MM calculations performed with a chloroform solvent model. Force field: a) MM3* (N–N distance = 10.10 Å, $H7_{lig}$-$H6_{endo,rec}$ = 5.40 Å, $H7_{lig}$-$H1_{rec}$ = 4.10 Å), b) MMFFs (N–N distance = 9.11 Å, $H7_{lig}$-$H6_{endo,rec}$ = 3.19 Å, $H7_{lig}$-$H1_{rec}$ = 3.39 Å), c) OPLS3e (N–N distance = 9.47 Å, $H7_{lig}$-$H6_{endo,rec}$ = 2.56 Å, $H7_{lig}$-$H1_{rec}$ = 3.99 Å).

force fields predict different orientations of the benzyl substituent, with the benzylic methylene group either pointing towards (MM3* and OPLS3e) or away (MMFFs) from the aromatic cavity of the receptor, and the phenyl group of the benzyl substituent oriented either towards or away from the aromatic cavity of the receptor (Figure 7). The MD simulation of complex **1·5** performed with the OPLS3e force field and a methanol solvent model shows the heptane chain of ligand **5** alternating between more or less extended conformations (N–N distance mainly between 9 and 10 Å) and the benzyl substituent having a lot of conformational freedom (Figure S87–88).

In conclusion, the MM calculations performed with the MM3* force field are in agreement with the experimental observation of an all-*anti* heptane chain of complex **1·5**. The MM calculations performed with the MM3* and OPLS3e force fields also places the methylene group of the benzyl substituent inside the aromatic cavity, which is consistent with the NMR data.

Conformation of complex 1·6

Due to severe overlap of several of the resonances of ligand **6**, interpretation of the NMR spectra is difficult. What can be observed is that when going from free to bound to receptor **1**, the resonance of H-4 of ligand **6** is displaced upfield by 0.84 ppm (Figure S50), suggesting that H-4 is situated inside or close to the aromatic cavity of receptor **1**. The ROESY spectrum of complex **1·6** (Figure S52) exhibits a weak cross peak between H-7 of the cyclohexyl substituent of ligand **6** and H-6_{endo}(H-12_{endo}) of receptor **1**, which is only possible if the cyclohexyl substituent is located somewhat inside the aromatic cavity of the receptor. The ROESY spectrum also shows cross peaks between H-1 and H-2, and H-1 and H-3 of the ligand, which could indicate *anti* interactions between C-1 and C-2, and C-2 and C-3 of the heptane chain of ligand **6**, although the overlap is too severe to draw any definite conclusions regarding the conformation of the rest of the heptane chain.

The energy-minimized conformations of complex **1·6** obtained from MM calculations using a chloroform solvent model and all three force fields exhibit two *gauche* interactions in the heptane chain of **6**, with N–N distances varying between 9.05 and 9.31 Å (Figure 8). The cyclohexyl substituent is oriented either towards (MM3* and OPLS3e, Figure 8a,c)) or away from (MMFFs, Figure 8b) the aromatic cavity of receptor **1**. The MD simulation of complex **1·6** performed with the OPLS3e force field and a methanol solvent model show a highly dynamic system, both in terms of the conformation of the heptane chain and the position of the cyclohexyl substituent, with the N–N distance varying between 8.5 and 10 Å and the cyclohexyl substituent moving between orientations more towards the receptor cavity and completely away from the cavity (Figure S89–90).

In conclusion, all force fields predict that the heptane chain of ligand **6** deviates from an all-*anti* conformation. The NMR data is insufficient to prove or disprove this prediction. The MM3* and OPLS3e force fields show that the cyclohexyl

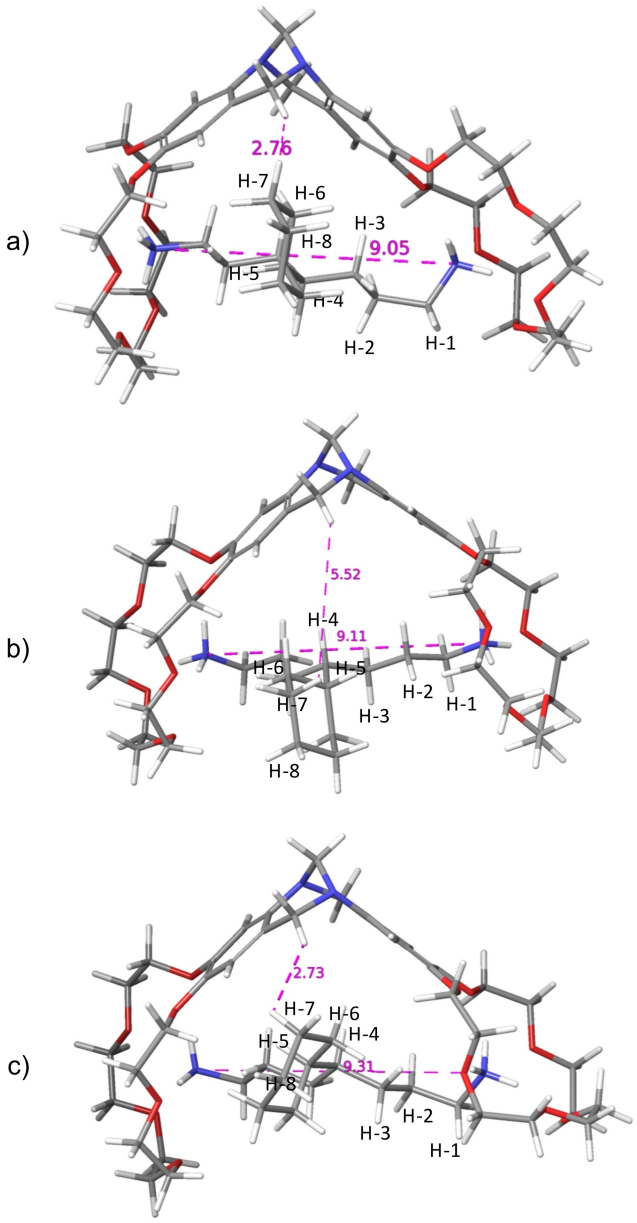

Figure 8. The lowest energy conformation of ligand **6** bound to receptor **1** from MM calculations performed with a chloroform solvent model. Force field: a) MM3* (N–N distance = 9.05 Å, $H7_{lig}$-$H6_{endo,rec}$ = 2.76 Å), b) MMFFs (N–N distance = 9.11 Å, $H7_{lig}$-$H6_{endo,rec}$ = 5.52 Å), c) OPLS3e (N–N distance = 9.31 Å, $H7_{lig}$-$H6_{endo,rec}$ = 2.73 Å).

substituent is oriented towards the aromatic cavity of receptor **1**, which is in agreement with the experimental findings.

Summary of the conformational analysis

An overview of the results from the conformational analysis of ligands **2–6**, both in solution and bound to receptor **1**, is presented in Table 6.

For most of the ligands, the heptane backbone seems to prefer an all-*anti* conformation, both in solution and when bound to receptor **1**. The exception is cyclohexyl-substituted ligand **6**, which adopts conformations with several *gauche* interactions, both in solution and when bound to the receptor. As previously mentioned, if the heptane backbones of the ligands have the same conformation within the series of ligands, the $\Delta\Delta G^0$ values could be interpreted as a measurement of how strong the interaction of a "free" substituent would be with a "free" aromatic cavity of **1**, since the interactions common for all the heptane backbones would be cancelled out. From the conformational analysis presented in Table 6, it appears that for complexes **1·3** and **1·4**, the conformation of the heptane backbone is conserved upon complexation. This fact, together with the fact that the substituents are located inside or partly inside the receptor cavity, allows us to make a tentative statement that the calculated $\Delta\Delta G^0$ values in Table 3 for ligand **3** and **4** can be taken as a measurement of the binding energy between the methyl- and phenyl group, respectively, and the aromatic cavity. As previously mentioned, these values are also in reasonable agreement with values of similar interactions determined by Wilcox torsion balance.[29,30]

With regard to the substituents, the experimentally determined conformations echo what was found quantitively in the relative binding energies. The methyl- and phenyl-substituted

Table 6. Summary of the conformational analysis of ligands **2–6**, free and bound to receptor **1**, based on NMR studies and molecular modelling. *a* and *g* refer to the conformation around the C–C bonds of the heptane chain of the ligands (*a* = *anti*, *g* = *gauche*).

	NMR[a]	MM3*[b]	MMFFs[b]	OPLS3e[b]
Free **2** chain[c]	*aaaaaa*	*aaaaaa*	*aaaaaa*	*aaaaaa*
1·2 chain	*aaaaaa*	*aaaaaa*	*aaaaaa*	*aaaaaa*
Free **3** chain[c]	*aaggaa*	*aaaaaa*	*aaaaaa*	*aaaaaa*
1·3 chain	*aaaaaa* inside cavity	*aaaaaa* outside cavity	*aaaaaa* outside cavity	*aaaaaa* partly inside cavity
1·3 substituent				
Free **4** chain[c]	*aaaaaa*	*aaaaaa*	*aaaaaa*	*aaaagg*
1·4 chain	*aaaaaa* partly inside cavity	*aaaaaa* partly inside cavity	*aaaaga* partly inside cavity	*aaaaaa* partly inside cavity
1·4 substituent				
Free **5** chain[c]	*aaaaaa*	*aaaaaa*	*aaaaga*	*aaaggg*
1·5 chain	*aaaaaa* partly inside cavity[d,e]	*aaaaaa* partly inside cavity[d]	*aaagag* partly inside cavity[e]	*aagaga* partly inside cavity[d,e]
1·5 substituent				
Free **6** chain[c]	*aaggaa*	*aaagaa*	*aaagaa*	*aaagaa*
1·6 chain	Inconclusive partly inside cavity	*aaagag* partly inside cavity	*aaagag* outside cavity	*aaagag* partly inside cavity
1·6 substituent				

[a] Eluciated from ^{1}H NMR spectroscopy, NOESY and ROESY performed in $CDCl_3$/MeOH-d_4 1:1. [b] Lowest energy conformations obtained with a chloroform solvent model. [c] The conformational analysis of the free ligands is included in the Supporting Information. [d] Methylene part of the benzylic substituent inside aromatic cavity. [e] Part of the aromatic ring of the benzylic substituent inside aromatic cavity.

ligands (**3** and **4**), which were found to bind strongest to the receptor (Table 3), form fairly rigid complexes where the substituent is located inside or partly inside the aromatic cavity of the receptor (Table 6). The benzyl- and cyclohexyl-substituted ligands (**5** and **6**), which were found to bind weakest to the receptor (Table 3), form complexes where the substituent extend farther from the aromatic cavity of the receptor (Table 6). The relatively lower stability of these complexes can also be seen in the more apparent dynamic behavior of these complexes. As an example, the NMR data obtained for complex **1**·**5** suggests that the ligand adopts several different conformations on the NMR time scale.

Comparing the lowest energy conformations obtained from MM calculations with different force fields, the MM3* force field is most successful at correctly predicting the experimentally determined conformations of the heptane backbone (Table 6). The OPLS3e force field correctly predicts the position of the ligand substituent in relation to the receptor cavity in all four complexes (**1**·(**3**-**6**)), while the MM3* force field correctly predicts the position in all of the complexes except for complex **1**·**3**. The MMFFs force field is least successful at predicting the experimentally determined conformations, both of the heptane backbones and the substituents.

Conclusion

A model system consisting of an 18-crown-6 Tröger's base receptor (**1**) and a number of 4-substituted hepta-1,7-diyl bisammonium salts (**2–6**) has been used to study the interactions between non-polar side chains of peptides and the aromatic cavity of a protein. NMR titrations, both with a weakly coordinating monoammonium salt and with one of the bisammonium ligands as competitor, were conducted to determine absolute ($K^{bis}_{1\cdot x}$) and relative ($K^{bis}_{1\cdot x}/K^{bis}_{1\cdot 2}$) association constants, as well as binding energies ($\Delta\Delta G^0_{1\cdot x-1\cdot 2}$, determined relative to the complex with unsubsituted ligand **2**). The $\Delta\Delta G^0_{1\cdot x-1\cdot 2}$ values suggested a weak but evident discrimination in the binding process based solely on the substituent on the ligand. Phenyl-substituted ligand **4** exhibited the strongest binding to receptor **1**, followed by methyl-substituted ligand **3**, unsubstituted ligand **2**, benzyl-substituted ligand **5** and cyclohexyl-substituted ligand **6**, with the corresponding $\Delta\Delta G^0_{1\cdot x-1\cdot 2}$ values ranging from -3.34 to 2.60 kJ mol^{-1}.

In addition to the quantitative NMR titration studies, NMR studies were conducted to determine the conformation of the ligands in solution and bound to the receptor. The results matched the observed trends from the relative binding energies, with ligands **3** and **4** forming more rigid complexes with the receptor and the substituent inside or in close contact with the cavity of the receptor, while the complexes with ligand **5** and **6** exhibited a more dynamic behaviour with more conformational freedom.

The obtained quantitative and qualitative experimental results were then used to compare and evaluate different computational methods. MM calculations were performed with three different force fields (MM3*, MMFFs and OPLS3e) and two different solvent models (chloroform and water) and the resulting energies were used to calculate $\Delta\Delta E^{MM}_{1\cdot x-1\cdot 2}$ values. The most acccurate prediction of the binding affinity of the different ligands (**2–6**) to receptor **1**, both in terms of absolute values and in terms of the ranking of the binding of the ligands to the receptor, was obtained with the MM3* force field and a chloroform solvent model. It was concluded that a chloroform solvent model worked better as an approximation of the experimental conditions ($CDCl_3$/MeOH-d_4 1:1) than a water solvent model. The introduction of a Boltzmann correction term did not improve the accuracy of the predictions.

Somewhat surprisingly, DFT calculations for the same systems resulted in substantially less accurate relative binding affinities than what was obtained from the best MM calculations. We note that the non-bonded interactions determining the relative binding strength is a composite of van der Waals interactions and solvation. These interactions are not solely calculated by the DFT method itself, but include contributions from add-on models for London dispersion and continuum solvation. The balance is heavily dependent on choice of functional and basis set. We chose combinations that are generally considered sufficiently accurate for applications in organic chemistry. The current results show that the chosen combination is insufficiently accurate for supramolecular interactions of the types found in biomolecules. The data derived here could be a valuable addition to existing data sets for future validation of computational methods in this field.

A qualitative analysis of the ability of the different force fields (MM3*, MMFFs and OPLS3e) to predict the experimentally determined conformation of the ligands in solution and when bound to the receptor revealed that the MM3* force field was most successful at predicting the conformation of the heptane backbone of the ligands, while the OPLS3e force field most correctly predicted the position of the substituents in relation to the receptor cavity. The conformational analyses were further supported by MD simulations.

The combination of techniques has allowed us to tentatively estimate the free binding energy of a methyl group and a phenyl group to an aromatic cavity, via CH-π (complex **1**·**3**), and combined aromatic-CH-π and π-π interactions (complex **1**·**4**), respectively. The values of -1.7 and -3.3 kJ mol^{-1} are in reasonable agreement with values of the CH-π and aromatic-CH-π interactions determined by Wilcox torsional balance,[29,30] taking into account the additional π-π contribution added to the latter interaction in our case, and the different contribution from solvophobic effects in our case compared to Wilcox's.

In conclusion, we have developed a model system to study peptide-protein interactions and generated qualitative and quantitative experimental data which can be used to benchmark different computational methods.

Acknowledgements

B.Sc. Susanne Henriksson and Dr Peter Michelsen, Amersham Health R&D, Malmö are thanked for the recording of ES-mass spectra. K.W thanks the Swedish Research Council, the Royal

Physiographic Society in Lund, the Crafoord Foundation, and the Swedish Foundation for Strategic Research for financial support.

Conflict of Interest

The authors declare no conflict of interest.

Keywords: computational chemistry · host–guest systems · NMR spectroscopy · NMR titrations · peptide-protein interactions

[1] M. A. Williams in *Protein-Ligand Interactions: Methods and Applications* (Eds.: M. A. Williams, T. Daviter), Humana Press, Totowa, NJ, **2013**, p. 3–34.
[2] X. Du, Y. Li, Y.-L. Xia, S.-M. Ai, J. Liang, P. Sang, X.-L. Ji, S.-Q. Liu, *Int. J. Mol. Sci.* **2016**, *17*, 144.
[3] T. Cserháti, M. Szögyi, *Peptides* **1995**, *16*, 165–173.
[4] C. A. Hunter, J. K. M. Sanders, *J. Am. Chem. Soc.* **1990**, *112*, 5525–5534.
[5] C. A. Hunter, K. R. Lawson, J. Perkins, C. J. Urch, *J. Chem. Soc. Perkin Trans. 2* **2001**, 651–669.
[6] E. A. Meyer, R. K. Castellano, F. Diederich, *Angew. Chem. Int. Ed.* **2003**, *42*, 1210–1250; *Angew. Chem.* **2003**, *115*, 1244–1287.
[7] S. K. Burley, G. A. Petsko, *Science* **1985**, *229*, 23.
[8] G. B. McGaughey, M. Gagné, A. K. Rappé, *J. Biol. Chem.* **1998**, *273*, 15458–15463.
[9] Y. Umezawa, S. Tsuboyama, H. Takahashi, J. Uzawa, M. Nishio, *Bioorg. Med. Chem.* **1999**, *7*, 2021–2026.
[10] M. Nishio, Y. Umezawa, M. Hirota, Y. Takeuchi, *Tetrahedron* **1995**, *51*, 8665–8701.
[11] M. Brandl, M. S. Weiss, A. Jabs, J. Sühnel, R. Hilgenfeld, *J. Mol. Biol.* **2001**, *307*, 357–377.
[12] R. L. Stanfield, I. A. Wilson, *Curr. Opin. Struct. Biol.* **1995**, *5*, 103–113.
[13] M. J. J. M. Zvelebil, J. M. Thornton, *Q. Rev. Biophys.* **1993**, *26*, 333–363.
[14] G. R. Marshall, *Curr. Opin. Struct. Biol.* **1992**, *2*, 904–919.
[15] V. Neduva, R. B. Russell, *Curr. Opin. Biotechnol.* **2006**, *17*, 465–471.
[16] E. Petsalaki, R. B. Russell, *Curr. Opin. Biotechnol.* **2008**, *19*, 344–350.
[17] J. Vagner, H. Qu, V. J. Hruby, *Curr. Opin. Chem. Biol.* **2008**, *12*, 292–296.
[18] J. Wang, Q. Shao, B. P. Cossins, J. Shi, K. Chen, W. Zhu, *J. Biomol. Struct. Dyn.* **2016**, *34*, 163–176.
[19] G. Vettoretti, E. Moroni, S. Sattin, J. Tao, D. A. Agard, A. Bernardi, G. Colombo, *Sci. Rep.* **2016**, *6*, 23830.
[20] S. A. Adcock, J. A. McCammon, *Chem. Rev.* **2006**, *106*, 1589–1615.
[21] I. Johansson-Åkhe, C. Mirabello, B. Wallner, *Sci. Rep.* **2019**, *9*, 4267.
[22] N. Sylvetsky, *Sci. Rep.* **2020**, *10*, 9218.
[23] R. A. Mata, M. A. Suhm, *Angew. Chem. Int. Ed.* **2017**, *56*, 11011–11018; *Angew. Chem.* **2017**, *129*, 11155–11163.
[24] Ö. V. Rúnarsson, J. Artacho, K. Wärnmark, *Eur. J. Org. Chem.* **2012**, *2012*, 7015–7041.
[25] J. C. Adrian, C. S. Wilcox, *J. Am. Chem. Soc.* **1989**, *111*, 8055–8057.
[26] A. P. Hansson, P.-O. Norrby, K. Wärnmark, *Tetrahedron Lett.* **1998**, *39*, 4565–4568.
[27] M. Bhaskar Reddy, M. Shailaja, A. Manjula, J. R. Premkumar, G. N. Sastry, K. Sirisha, A. V. S. Sarma, *Org. Biomol. Chem.* **2015**, *13*, 1141–1149.
[28] S. Paliwal, S. Geib, C. S. Wilcox, *J. Am. Chem. Soc.* **1994**, *116*, 4497–4498.
[29] E.-i. Kim, S. Paliwal, C. S. Wilcox, *J. Am. Chem. Soc.* **1998**, *120*, 11192–11193.
[30] B. Bhayana, C. S. Wilcox, *Angew. Chem. Int. Ed.* **2007**, *46*, 6833–6836; *Angew. Chem.* **2007**, *119*, 6957–6960.
[31] F. Jensen, *Introduction to Computational Chemistry*, 2nd ed., Wiley, Weinheim, **2017**, p. 22–77, 232–264.
[32] C. J. Pedersen, *J. Am. Chem. Soc.* **1967**, *89*, 7017–7036.
[33] A. Marmur, *J. Am. Chem. Soc.* **2000**, *122*, 2120–2121.
[34] C. S. Wilcox, in *Frontiers in Supramolecular Organic Chemistry and Photochemistry* (Eds.: H.-J. Scheider, H. Durr), Weinheim, New York, **1991**, p. 123–143.
[35] L. Fielding, *Tetrahedron* **2000**, *56*, 6151–6170.
[36] K. Hirose, *J. Inclusion Phenom. Macrocyclic Chem.* **2001**, *39*, 193–209.
[37] P. Thordarson, *Chem. Soc. Rev.* **2011**, *40*, 1305–1323.
[38] F. G. J. Odille, S. Jónsson, S. Stjernqvist, T. Rydén, K. Wärnmark, *Chem. Eur. J.* **2007**, *13*, 9617–9636.
[39] P. Job, *Ann. Chim.* **1928**, *9*, 109–123.
[40] R. Sahai, G. L. Loper, S. H. Lin, H. Eyring, *Proc. Natl. Acad. Sci. USA* **1974**, *71*, 1499–1503.
[41] N. Schulz, S. Schindler, S. M. Huber, M. Erdelyi, *J. Org. Chem.* **2018**, *83*, 10881–10886.
[42] B. J. Whitlock, H. W. Whitlock, *J. Am. Chem. Soc.* **1990**, *112*, 3910–3915.
[43] MM3* refers to the MM3 force field implemented in Macro-Model.
[44] N. L. Allinger, Y. H. Yuh, J. H. Lii, *J. Am. Chem. Soc.* **1989**, *111*, 8551–8566.
[45] T. A. Halgren, *J. Comput. Chem.* **1999**, *20*, 720–729.
[46] K. Roos, C. Wu, W. Damm, M. Reboul, J. M. Stevenson, C. Lu, M. K. Dahlgren, S. Mondal, W. Chen, L. Wang, R. Abel, R. A. Friesner, E. D. Harder, *J. Chem. Theory Comput.* **2019**, *15*, 1863–1874.
[47] E. Harder, W. Damm, J. Maple, C. Wu, M. Reboul, J. Y. Xiang, L. Wang, D. Lupyan, M. K. Dahlgren, J. L. Knight, J. W. Kaus, D. S. Cerutti, G. Krilov, W. L. Jorgensen, R. Abel, R. A. Friesner, *J. Chem. Theory Comput.* **2016**, *12*, 281–296.
[48] F. Mohamadi, N. G. J. Richards, W. C. Guida, R. Liskamp, M. Lipton, C. Caufield, G. Chang, T. Hendrickson, W. C. Still, *J. Comput. Chem.* **1990**, *11*, 440–467.
[49] MacroModel, Schrödinger, LLC, New York, NY, 2020. Schrödinger release 2020–3.
[50] T. Liljefors, P.-O. Norrby, I. Pettersson, in *Computational Medicinal Chemistry for Drug Discovery* (Eds.: P. Bultinck, H. De Winter, W. Langenaeker, J. P. Tollenaere), Marcel Dekker, New York, **2004**, p. 1–28.
[51] Y. Zhao, D. G. Truhlar, *Theor. Chem. Acc.* **2008**, *120*, 215–241.
[52] J.-D. Chai, M. Head-Gordon, *Phys. Chem. Chem. Phys.* **2008**, *10*, 6615–6620.
[53] C. M. Cortis, R. A. Friesner, *J. Comput. Chem.* **1997**, *18*, 1570–1590.
[54] D. Neuhaus, M. P. Williamson, The Nuclear Overhauser Effect in Structural and Conformational Analysis, 2nd ed., Wiley, Weinheim, **2000**.

Manuscript received: March 10, 2021
Accepted manuscript online: April 28, 2021
Version of record online: June 25, 2021

